Accepted Manuscript

International Journal of Structural Stability and Dynamics

Article Title:	Experimental and Numerical Study of Basalt FRP Strip Strengthened RC Slabs under Impact Loads
Author(s):	Wensu Chen, Thong M. Pham, Mohamed Elchalakani, Huawei Li, Hong Hao, Li Chen
DOI:	10.1142/S0219455420400015
Received:	07 June 2019
Accepted:	15 October 2019
To be cited as:	Wensu Chen *et al.*, Experimental and Numerical Study of Basalt FRP Strip Strengthened RC Slabs under Impact Loads, *International Journal of Structural Stability and Dynamics*, doi: 10.1142/S0219455420400015
Link to final version:	https://doi.org/10.1142/S0219455420400015

Experimental and Numerical Study of Basalt FRP Strip Strengthened RC Slabs under Impact Loads

Wensu Chen[1], Thong M. Pham[1], Mohamed Elchalakani[2,*], Huawei Li[1], Hong Hao[1,*], and Li Chen[3]

[1] Centre for Infrastructural Monitoring and Protection, School of Civil and Mechanical Engineering, Curtin University, Australia

[2] School of Civil, Environmental and Mining Engineering, the University of Western Australia, Australia

[3] School of Civil Engineering, Southeast University, Nanjing, China

*Corresponding authors

Abstract

Basalt fiber reinforced polymer (BFRP) has been applied for strengthening concrete structures. However, studies on reinforced concrete (RC) slabs strengthened by BFRP strips under impact loads are limited in open literature. This study investigates the efficiency of using BFRP strips with various strengthening layouts and anchoring schemes on the impact resistance of RC slabs. A total of 11 two-way square slabs were prepared and tested, including one reference specimen without strengthening and ten slabs strengthened with BFRP strips and/or anchors. The RC slabs were impacted by a drop weight with increasing height until slab failure. The observed failure modes include punching shear failure, BFRP sheet debonding and reinforcement fracture. The failure modes and the effects of using various strengthening schemes on the impact resistant capacity of RC slabs were examined. The quantitative measurements such as impact velocity, indentation depth and diameter were compared and

discussed. In addition, numerical studies were carried out by using LS-DYNA to simulate the impact tests of RC slabs with and without BFRP strengthening. With the calibrated numerical model, the impact behavior of slabs with various dimensions and strengthening layouts under different impact intensities can be predicted with good accuracy.

Keywords: Basalt fiber reinforced polymer (BFRP); strengthening; RC slab; anchor; impact load

1. Introduction

Reinforced concrete (RC) slabs may be subjected to impact loadings such as falling objects from the upper floor [1] and falling rocks on rock sheds [2, 3]. Under impact loading, the performance of RC slabs differs from that under static loading owing to the strain rate effect and inertial effect [4, 5]. Therefore, a few studies about the slabs under impact loads have been conducted to examine their failure mode and impact resistant capacity [5-8]. Xiao et al [5, 6] investigated the behavior of RC slabs under drop weight impact by considering various impact energy, loading rate, impacted area, slab depth and reinforcement ratios. It was found that the punching shear failure was a typical failure mode of RC slabs which can be resisted by the longitudinal and shear reinforcements. However, the shear reinforcements provided more contribution to the impact resistance capacity of RC slabs than the longitudinal reinforcements. Micallef et al. [7] reported that punching shear capacity of RC slab was enhanced with the increase of loading rate due to the inertial effect and strain rate effect. Zineddin and Krauthammer [8] investigated the dynamic response of RC slabs with different types of reinforcements under various impact energies. The test results showed that the reinforcement

configurations significantly affected the failure modes of RC slabs, which was similar to the observation by Otham and Marzouk [9]. Moreover, in order to improve the impact resistant capacity of RC slabs, steel fiber concrete [10], high strength concrete [9] and ultra-high performance fiber-reinforced concrete [11] were used for the RC slabs. The steel fibers and high-performance concrete can increase the impact resistance capacity, suppress concrete cracks and reduce local damages of slabs under impact loads.

Strengthening techniques such as using fiber reinforced polymer (FRP) strips were effective to improve impact resistance capacity of RC slabs [12, 13]. FRP is made from polymer matrix reinforced with high strength fibers [14]. It has been widely used to strengthen RC structures owing to its superiorities such as high tensile strength, low weight and good resistance to corrosion [15-20]. The commonly used FRP composites include aramid FRP (AFRP), basalt FRP (BFRP), carbon FRP (CFRP) and glass FRP (GFRP). To date, there are limited studies of RC slabs strengthened with CFRP sheets under impact loads [12, 13, 21, 22]. It was reported that using CFRP can improve impact resistance capacity of RC slabs. Basalt FRP as an alternative material for RC slab strengthening is less investigated. In addition, premature FRP debonding due to localized flexural or shear-flexural cracks undermined the strengthening effectiveness and lowered the utilization efficiency of FRP material [23, 24]. In order to prevent the premature debonding of FRP, various anchorage systems were used [24, 25]. However, the effectiveness of using the anchorage system including anchor plates and Mason bolts on the impact resistance capacity of strengthened slabs has not been investigated.

In this study, one reference two-way RC slab without strengthening and ten RC slabs

strengthened with BFRP strips of various strengthening schemes and anchorage systems were prepared and tested by using drop weight testing system. The failure modes were observed and the effect of using different strengthening schemes on impact resistant capacity of RC slabs was examined. The indentation depth and diameter were measured and compared. In addition, numerical models were developed by using LS-DYNA to simulate impact behaviors of RC slabs with or without BFRP strengthening.

2. Experimental program

2.1. Testing specimens

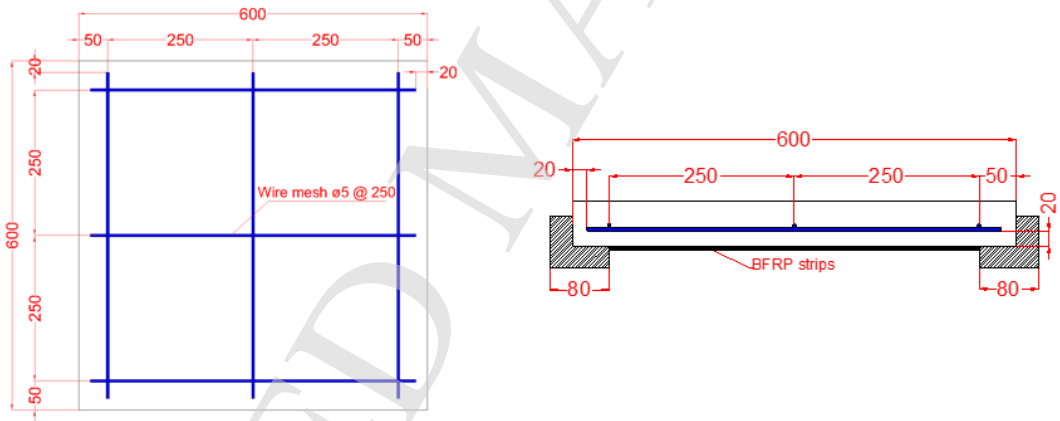

Figure 1. Dimension and reinforcement configuration of RC slab (Unit: mm) (L) Plan view; (R) Elevation view;

A total of 11 square two-way RC slabs including one reference RC slab and ten BFRP strengthened slabs with different strengthening schemes were prepared. The geometric dimension and reinforcement configuration of the RC slabs are shown in Figure 1. The dimension of the tested square slabs was 600 mm in width and 60 mm in depth. The free span of the slabs was 500 mm in both directions. The RC slabs were reinforced with the steel wire

mesh of 5 mm in diameter at the space of 250 mm. The wire mesh was placed at the tension side with 20 mm concrete cover. The yield strength and Young's modulus of the steel reinforced wire mesh were 500 MPa and 200 GPa, respectively. The concrete compressive strength was measured as 36.4 MPa after 28 days.

A total of six strengthening schemes employed in this study are illustrated in Figure 2. All strengthening schemes were designed with four layers of BFRP strips at the tension side of slabs. For example, there are two layers in X direction and two layers in Y direction for the strengthening scheme A; the strengthening scheme F has two layers in 45 degree diagonal direction and two layers in -45 degree diagonal direction. In addition, anchor bolts and plates were considered in the strengthening schemes B and D to investigate the effect of anchorage on their strengthening efficiency. The RC slabs with different BFRP strengthening schemes are detailed in Table 1.

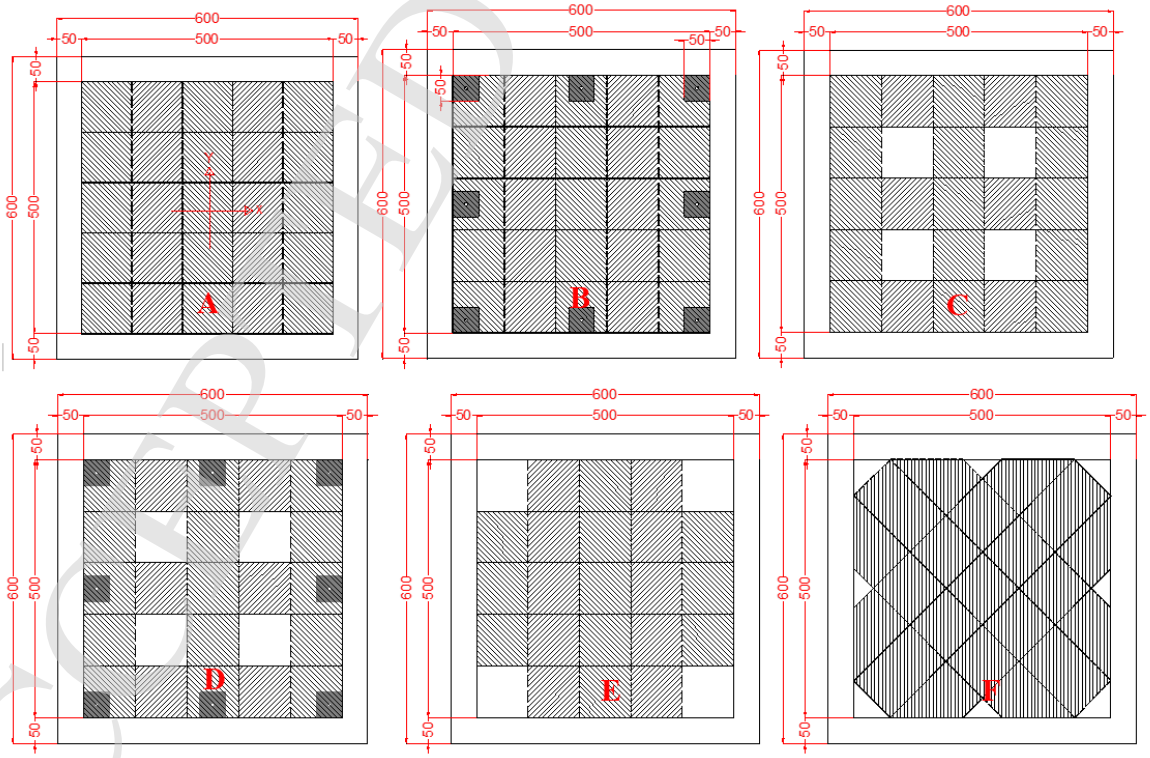

Figure 2. Strengthening schemes A/B/C/D/E/F (Unit: mm)

Table 1. Description of test scheme and strengthening scheme

Specimen	Drop height (m)	Strengthening scheme	Strengthening scheme description
S1	1.5	N/A	Reference specimen without strengthening
S2	1.5	A	Two layers (10 BFRP strips) in X direction and two layers (10 BFRP strips) in Y direction for the whole area
	2.0		
S10	2.0		
S4	2.5		
S3	1.5	B	Strengthening scheme A + anchors
	2.0		
S5	1.5	C	Two layers (6 BFRP strips) in X direction and two layers (6 BFRP strips) in Y direction at the space of 100 mm
S7	2.5		
S6	1.5	D	Strengthening scheme C + anchors
S8	1.5	E	Two layers (6 BFRP strips) in X direction and two layers (6 BFRP strips) in Y direction at the centre of slab
S11	2.5		
S9	1.5	F	Two layers (6 BFRP strips) in each diagonal direction
	2.0		

2.2. BFRP and anchorage system application

2.2.1. BFRP material and application

Unidirectional BFRP strips with width of 100 mm and length of 500 mm were used to strengthen RC slabs in this study. The unit weight of BFRP strip was 300 g/m^2 and its nominal thickness was 0.12 mm [14]. In accordance with ASTM [26], material properties of BFRP strip were determined by conducting BFRP coupon tensile tests. The BFRP strips had tensile strength of 1642.2 MPa, Young's modulus of 77.9 GPa, and rupture strain of 2.1% [14]. The BFRP strips were attached to the tension side of RC slabs by using epoxy resin which was a mixture of resin and hardener (West System 105 and 206) at a ratio of 5:1. The ultimate tensile strength, elastic modulus and rupture tensile strain of epoxy resin were 50.5 MPa, 2.8 GPa and 4.5%,

respectively. The strengthening effectiveness was greatly affected by the quality of concrete surface preparation and BFRP strips installation. In order to ensure the bonding of BFRP strips, the concrete substrate was pretreated by using a needle scaler to remove the weak mortar and dust particles were cleaned before applying the adhesive as shown in Figure 3 (L). The adhesive was applied as a primer before applying the first layer of BFRP strips and adhesive. A roller was used to remove the air bubbles by rolling the BFRP strips, followed by another layer of BFRP strip applied in another direction.

Figure 3. (L) Preparation of concrete surface before applying BFRP strips; (R) Anchor bolt and plate

2.2.2. Anchorage system application

The specimen S3 with strengthening scheme B and the specimen S6 with strengthening scheme D were equipped with anchorage systems. The anchorage systems consisted of anchor plates and Mason bolts. The dimension of the square anchor plate was 50 by 50 mm. The steel plates were fastened at the specific locations along the slab boundary by using 6.5 mm diameter Mason bolts with the depth of 36 mm. The installed anchorage component is shown in Figure 3 (R).

2.3 Test setup and instrumentation

Impact tests were conducted by using a drop weight impact system as shown in Figure 4. The slab specimens were placed over the steel support on four edges and fixed by eight G-clamps around four corners to provide vertical restraints and prevent the upward movement of the slabs during the impact tests. The steel drop weight of 108 kg was lifted up to the desired height and released freely through a cylindrical guide tube and then impacted onto the top surface of the tested slabs at mid-span. The hemispherical drop weight has the flat impact head with the diameter of 100 mm. The dimensions of the drop weight are given in Figure 4. The drop height was summarized in Table 1. In order to achieve complete failure of RC slabs, e.g., concrete scabbing, reinforcement fracture or debonding of BFRP sheet, some specimens were subjected to repeated impact loads by increasing the drop heights as given in Table 1. For example, the specimen S2 was sequentially impacted by the drop heights of 1.5 m and 2.0 m. The specimen experienced slight concrete damage after the first impact and then suffered complete failure after the second impact. The FASTCAM SA-Z high-speed camera was used to capture the whole impact process of slab failure. In addition, tracking points were attached onto the drop weight as shown in Figure 4, which enabled the high-speed camera to capture the velocity and displacement of drop weight. After impact, the dimension of indentation area (i.e., diameter and depth) of slabs was measured and compared.

Figure 4. Test setup and drop weight (all dimension in mm)

3. Experimental results and discussions

A total of 11 RC slabs were impacted by the drop weight released from different heights until complete failure of RC slabs. Their impact resistant capacities were analyzed and discussed. The testing data of RC slabs are summarized in Table 2. The impact velocities were extracted from high speed camera clips. The indentation depth and diameter on the top surface of RC slabs were compared to illustrate the damage of each specimen.

Table 2. Summary of testing data

Specimen	Strengthening scheme	Impact No.	Drop height (m)	Impact velocity (m/s)	Indentation depth (mm)	Indentation diameter (mm)
S1	N/A	1	1.5	5.4	100.0	440
S2	A	1	1.5	5.4	4.0	*
		2	2.0	5.9	△	△
S10		1	2.0	5.8	30.0	400
S4		1	2.5	6.9	65.0	370
S3	B	1	1.5	5.2	7.0	*
		2	2.0	6.2	△	△
S5	C	1	1.5	4.8	3.0	190
S7		1	2.5	#	40.0	450
S6	D	1	1.5	5.1	5.0	180

S8	E	1	1.5	5.2	20.0	140
S11		1	2.5	6.8	△	△
S9	F	1	1.5	5.3	15.0	155
		2	2.0	6.2	△	△

Note: * Insignificant indentation was not measured; △ Indentation was not measured due to total failure; # Impact velocity was not reliably obtained.

3.1. Reference specimen

The reference specimen S1 without BFRP strengthening was impacted from the drop height of 1.5 m with the impact velocity of 5.4 m/s. The failure mode of the reference specimen is shown in Figure 5. It was observed that RC slab without strengthening scheme suffered severe punching shear and fracture of reinforcement. The severe punching shear damages caused complete failure of the slab such as concrete spalling at the impact zone, concrete scabbing on the bottom surface and reinforcement fracture. As shown in Figure 5(a), concrete cracks propagated from the impact zone to clamp constraints on the top surface of the slab. In addition, the impact load resulted in the concrete scabbing on the bottom surface of the slab as shown in Figure 5(b). The punching shear cone broke into several parts and the reinforcement wire mesh fractured at the mid-span of the slab. In addition, the maximum indentation depth and diameter was about 100 mm and 440 mm, respectively.

(a) Top surface (b) Bottom surface

Figure 5. Failure mode of reference specimen S1

3.2. Effect of different BFRP strengthening layouts

Four types of BFRP strengthening layouts were used to strengthen the RC slabs as shown in Figure 2, i.e., strengthening the whole area (strengthening scheme A), strip strengthening at a space of 100 mm (strengthening scheme C), strengthening along orthogonal directions at the centre of slab (strengthening scheme E), and strengthening along diagonal directions (strengthening scheme F). The specimens S2, S5, S8 and S9 corresponding to the strengthening layout A/C/E/F were tested under the impact with drop height of 1.5 m to investigate the effect of BFRP strengthening layout on the impact resistance of the slabs. Figure 6 shows the failure modes of the RC slabs strengthened with different BFRP strengthening layouts. The specimen S2 (strengthening scheme A) experienced no obvious indentation, concrete spalling and scabbing under the impact load. Radial cracks were observed on the top surface and some fine cracks initiated from the impact zone to the boundaries of the slab. As shown in Figure 6 (b), the specimen S5 (strengthening scheme C) experienced concrete spalling and debonding of BFRP sheet. On the top surface of specimen S5, the concrete spalling was observed at the impact zone and some concrete cracks extended to the G-clamps and boundaries, indicating

flexural failure mode. In addition, the circumferential cracks were observed on the top surface of the slab, indicating punching shear failure mode. The indentation depth and diameter of specimen S5 at mid-span was about 3 mm and 190 mm, respectively. As observed from the bottom surface, the BFRP sheet was debonded from the RC slab along the boundaries. The specimen S8 (strengthening scheme E) strengthened at the centre of the slab in orthogonal direction experienced punching shear failure and debonding of BFRP sheet as shown in Figure 6 (c). The significant circumferential cracks were observed close to the impact zone on the top surface. The inclined cracks propagated from the impact zone to the G-clamps. The debonded BFRP sheet pulled out the concrete punching shear cone at mid-span, resulting in the exposure of reinforcement wire mesh. The slab showed a damaged area with indentation depth of 20 mm and indentation diameter of 140 mm. For the specimen S9 (strengthening scheme F), concrete spalling occurred at the impact zone, resulting in small concrete circumferential cracks. The dimension of the indentation was 15 mm in depth and 155 mm in diameter. Some severe circumferential cracks were formed near the boundaries of the slab due to the flexural and shear actions. No obvious debonding of BFRP sheet was observed from the bottom surface of the slab. It can be concluded that using BFRP can effectively enhance the impact resistance of RC slabs and suppress the development of concrete cracks as compared with the reference specimen S1. However, different strengthening layouts demonstrated various strengthening efficiency to resist drop weight impact. Strengthening scheme A (using 10 BFRP strips in one direction), was very effective to mitigate the damage of slabs and suppress the number and width of the concrete cracks induced by impact loads. With respect to three BFRP strengthening layouts (i.e.

C/E/F) using 6 BFRP strips in one direction, strengthening scheme E had the lowest strengthening efficiency and the scheme F had the best performance in suppressing concrete cracks and minimizing the crack width.

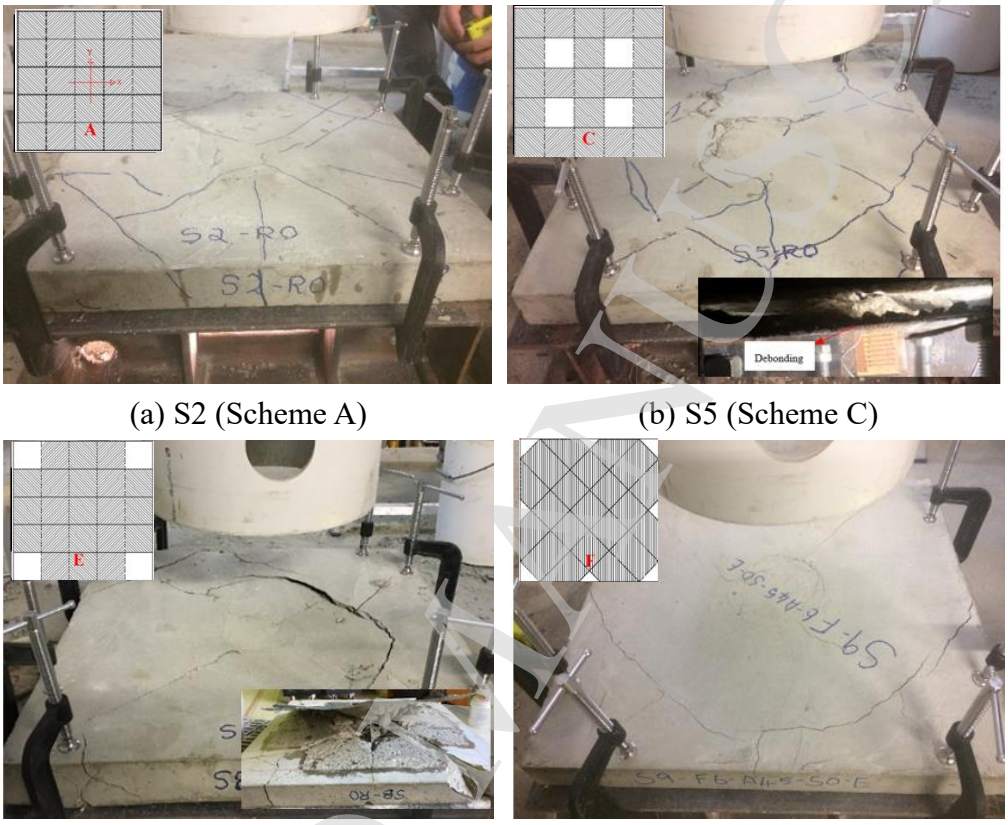

(a) S2 (Scheme A) (b) S5 (Scheme C)

(c) S8 (Scheme E) (d) S9 (Scheme F)

Figure 6 Failure modes of RC slabs with different BFRP layouts (1.5 m drop height)

3.3. Effect of anchor

To investigate the effect of anchors on the strengthening performance, the specimens S3 and S6 were prepared with the strengthening scheme of B and D, respectively. A total of eight Mason bolts along with anchor plates were installed on the slabs. The failure modes of S3 and S6 under the drop weight impact with drop height of 1.5 m shown in Figure 7 were compared with the failure modes of S2 and S5 as shown in Figure 6. Concrete cracks extending from the impact zone to the G-clamps were observed on the top surface of the specimen S3 after the

impact as shown in Figure 7 (a). Limited concrete cracks distributed along the boundaries on the top surface and the indentation was not evident. It is worth noting that cracks close to the drilled anchor holes were observed, indicating that the anchor holes produced additional concrete cracks as compared to the specimen S2 without anchorage system, probably owing to stress concentration. As shown in Figure 7 (b), the specimen S6 experienced the debonding of BFRP sheets, which was similar to the failure mode of the specimen S5. In addition, the anchor bolts at the middle of the boundary were detached from the BFRP sheet and concrete slab due to tensile stress wave under impact loading. As observed, no concrete punching shear cone was pulled out at the middle of the bottom surface, which was different from the failure mode of specimen S5. The indentation depth and diameter of specimens S6 were 5 mm and 180 mm, respectively, which were similar to 3 mm and 190 mm of specimen S5. Therefore, using anchor systems along with BFRP strengthening reduced the concrete scabbing on the bottom surface but did not significantly mitigate concrete cracks on the top surface as compared with the RC slab only strengthened by BFRP sheets. This is because using anchors enhanced the bonding between RC slab and BFRP sheet, while the anchor holes weakened the strength of the slabs to a certain extent and thus mitigated the strengthening efficiency.

(a) S3 (Scheme B) (b) S6 (Scheme D)

Figure 7. Failure modes of slabs strengthened with anchors

3.4. Effect of impact energy

In order to investigate the effect of impact energy on the performance of RC slab strengthened with different BFRP strengthening layouts, the specimens S2, S3 and S9 were impacted twice with the drop height of 1.5 m and 2.0 m. Figure 8 shows the failure mode of RC slabs with different strengthening layouts under repeated impacts. It can be seen that the specimens S2, S3 and S9 presented slight radial cracks and circumferential cracks under the first impact with the drop height of 1.5 m due to global flexural mode. The indentation diameters of the specimens S2 and S3 were not measured due to their insignificant indentation at the impact zone while the indentation diameter of the specimen S9 was 155 mm, indicating that the RC slab strengthened by the whole area was more robust than the slabs strengthened along two diagonal directions under the first impact. The local punching shear failure and the debonding failure of BFRP sheet were not observed in these specimens under the first impact. However, under the second impact with the drop height of 2.0 m, all three specimens could not survive and broke into several pieces. In addition, the reinforcement wire mesh in the slabs fractured and BFRP sheets were detached from the bottom surface of the RC slabs.

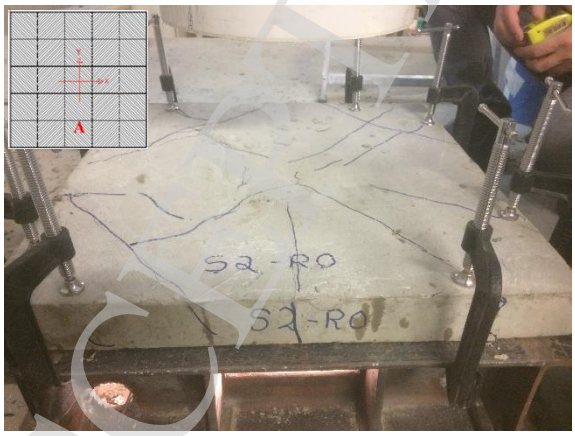

(a) S2 under the first impact

(b) S2 under the second impact

(c) S3 under the first impact

(d) S3 under the second impact

(e) S9 under the first impact

(f) S9 under the second impact

Figure 8. Failure mode of RC slabs under repeated impacts

In addition, three groups of specimens were tested by drop weight with different heights. Failure modes of the specimens are shown in Figure 9. For the first group, the specimens S2, S10 and S4 with the same strengthening scheme A were subjected to single impact with the drop height of 1.5 m, 2.0 m and 2.5 m, respectively. As shown in Figure 9 (a), with the increase of impact energy, the failure mode of the strengthened RC slabs changed from global flexural failure to local punching shear failure at the impact zone. The specimens S10 and S4 also experienced debonding failure of BFRP sheet, resulting in concrete scabbing on the bottom surface under the impact zone. For the second group, the specimens S5 and S7 with the same strengthening scheme C were impacted under the drop height of 1.5 m and 2.5 m, respectively. As shown in Figure 9 (b), the specimen S5 experienced concrete spalling at the impact zone

and debonding of BFRP sheet. Under the higher drop height of 2.5 m, the specimen S7 experienced significant punching shear failure at the impact zone. Concrete cracks extended from the impact zone to the boundaries. The concrete punching shear cone caused the debonding of BFRP sheet from the bottom surface of the slab. For the third group, the specimens S8 and S11 that strengthened with the BFRP strips orthogonally at the centre of the slab (strengthening scheme E) were impacted with the drop heights of 1.5 m and 2.5 m, respectively. As shown in Figure 9 (c), the specimen S8 experienced punching shear failure and debonding of BFRP sheet. The specimen S11 subjected to higher impact energy experienced the most severe damage among the specimens. The reinforcement wire mesh fractured and the BFRP sheets were debonded from the RC slab and towed out concrete at the impact zone. Therefore, it can be concluded that the RC slab strengthened with BFRP strips orthogonally at the centre is more vulnerable to the damage than the slabs strengthened with other strengthening schemes. With the increase of drop height, the indentation depth and diameter of these RC slabs increased as given in Table 2.

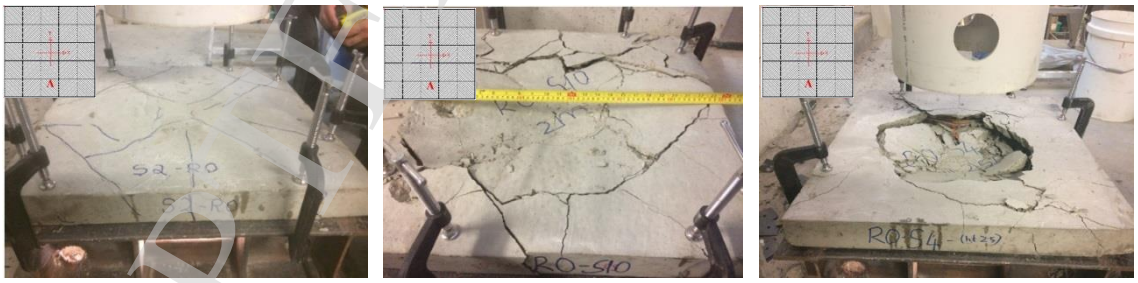

(a) S2-1.5 m (b) S10-2.0 m (c) S4-2.5 m

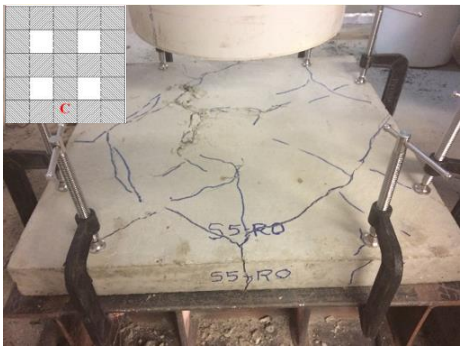

(d)S5-1.5 m

(e) S7-2.5 m

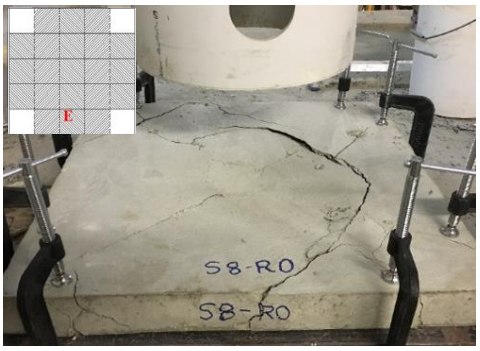

(f) S8-1.5m

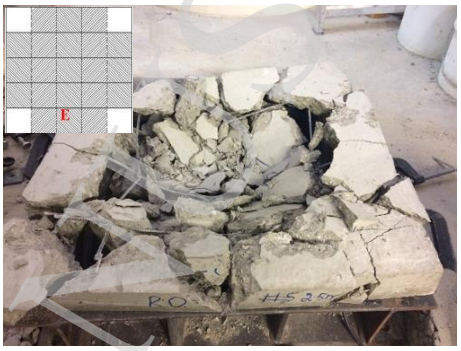

(g) S11-2.5 m

Figure 9 Failure modes of RC slabs impacted with different impact energy

3.5. Comparison and discussions

By observing concrete damage and crack pattern from the tested RC slabs, the failure mode was found to be greatly affected by the BFRP strengthening scheme and impact energy. The unstrengthened RC slab impacted by drop weight at height of 1.5 m experienced severe punching shear failure and fracture of wire mesh. The impact resistance capacity of RC slabs was enhanced by using different BFRP strengthening layouts. The strengthening efficiency was greatly affected by premature debonding of BFRP. As shown in Figure 6, premature debonding occurred in the slabs strengthened at the space of 100 mm (S5) and strengthened along orthogonal directions (S8) while the BFRP sheet was well attached to the bottom surface of the slabs strengthened for the whole area (S2) and strengthened along diagonal directions (S9). Therefore, the BFRP sheet layouts such as strengthening the whole area and strengthening along

diagonal directions can increase the integrity of slabs and limit the number and width of the concrete cracks in a more efficient way. The scheme of BFRP strengthening orthogonally at the centre of the slab has the lowest strengthening efficiency among the strengthening layouts considered in the study. With respect to the repeated impact scenario, the specimens S2, S3 and S9 experienced slight radial cracks and circumferential cracks under the first impact with drop height of 1.5 m. With the increase of impact energy, the failure mode of the RC slabs changed from global flexural failure to local punching shear failure. Under the second impact with drop height of 2.0 m, all three specimens experienced severe damages regardless of the strengthening layouts. In addition, the anchorage system cannot provide significant enhancement on the performance of RC slabs to resist drop weight impact. This is because the anchor holes weakened the strength of the slabs around these holes and thus induced concrete cracks, which resulted in the detachment of anchor bolts and plates.

As mentioned above, Basalt FRP is an alternative and cost-effective material for RC slab strengthening but less investigated. To the best of author's knowledge, there is no testing data available on BFRP sheet strengthened RC slab under impact load. The effects of using BFRP strengthening and anchorage systems on the impact resistance capacity of the slabs have not been investigated. However, there are limited studies on RC slabs strengthened with CFRP or AFRP strips under impact loads [12, 13, 22, 27]. Bhatti et al. [12] investigated the impact behaviors of RC slabs strengthened with CFRP and AFRP sheet under single and repeated impact loads. Two weaving methods of FRP strips to strengthen slabs, i.e., unidirectional and cross-directional weaving orthogonally, were compared. It was found that the strengthening

efficiency by using cross-directional weaving FRP sheet was better than that of unidirectional weaving due to the superior dispersion of tensile stress on the back surface of slab under impact loads. However, the strengthening schemes in orthogonal and diagonal directions and the strengthening schemes in concentrated and spaced distributions were not compared. Yılmaz et al [13] conducted experimental and numerical studies on the impact response of nine RC slabs orthogonally and diagonally strengthened by CFRP strips with spacing between strips in one and two directions. The slab diagonally strengthened with CFRP strips in two directions exhibited the best performance in mitigating concrete cracks and minimizing crack width, which is consistent with the observations in this study. However, the specimens only experienced cracking and no severe damage and no CFRP debonding was observed due to the low impact energy considered in the study. Radnić et al. [22] experimentally and numerically investigated impact behaviors of eight RC slabs with or without CFRP strips under 4 kg drop weight impact. It was reported that the relatively large space between CFRP strips considered in the study resulted in limited strengthening efficiency on the bearing capacity of RC slabs. Mutalib et al. [27] investigated the performance of four two-way slabs under repeated impact loads. Four slabs included one reference slab (S1), one slab (S2) strengthened with two layers of CFRP sheets at full area and two CFRP strengthened slabs (S3 and S4) with mechanical anchors applied along the slab boundary and the entire slab, respectively. It was observed that CFRP strengthening slab S2 experienced perforation and severe CFRP debonding under the second impact with the whole piece of CFRP sheet delaminated from the slab, as shown in Figure 10. The efficiency of CFRP strengthening was greatly undermined due to the severe

debonding of CFRP sheet. Therefore, the specimen S3 and S4 [27] applied with anchors showed much better impact resistance capacity than S2 by preventing premature debonding failure, which also demonstrated the effectiveness of using anchors in the enhancement of impact resistance. It should be noted that the failure mode of slab S2 in [27] was different from the failure mode of slab S2 with the similar strengthening scheme in this study, where the BFRP sheet was debonded from the slab with a thick layer of concrete substrate, indicating sufficient bond strength was provided between BFRP sheet and concrete substrate. It might be due to different concrete surface preparation before BFRP sheet installation or the used adhesive with different strength. Since debonding occurred inside concrete substrate in this study, anchors provided very limited efficiency in improving impact resistance. Conversely, the anchor holes might weaken the strength of the slabs and thereby undermine the strengthening efficiency. In addition, since no BFRP rupture was observed in the tests, there is probably no need to apply the FRP with higher tensile strength and cost such as CFRP for the slab strengthening in practice.

Figure 10 Failure modes of RC slabs strengthened with CFRP sheet (L) Perforation; (R) CFRP debonding [28]

4. Numerical simulations

To further study the impact resistance of the slabs, numerical models were developed by

using the explicit finite element code LS-DYNA to simulate the impact tests on the RC slabs with and without BFRP strengthening strips. The numerical models were calibrated with the experimental data by comparing failure modes and quantitative results.

4.1. Finite element model

The 8-node constant stress solid element with single integration point was used to simulate the concrete, steel drop weight and steel support. The reinforcement wire mesh was simulated by the Hughes-Liu beam element with 2 × 2 Gauss quadrature integration. The 4-node Belytschko-Tsay shell element was employed to simulate the BFRP sheet. The mesh size of 10 mm was determined for the numerical model after conducting mesh sensitivity analysis to obtain reliable results with reasonable computational time. The numerical model has a total of 37,165 solid elements for the concrete slab, drop weight and steel support, 5000 shell elements for the BFRP strips, and 360 beam elements for the reinforcement wire mesh. The numerical model of RC slab strengthened by BFRP sheets is shown in Figure 10. In the numerical model, steel support was simplified as a rigid support. The nodes corresponding to the position of G-clamps were constrained on the top surface of the RC slab. A perfect bonding was assumed by sharing the same nodes at the identical locations between reinforcement wire mesh and surrounding concrete.

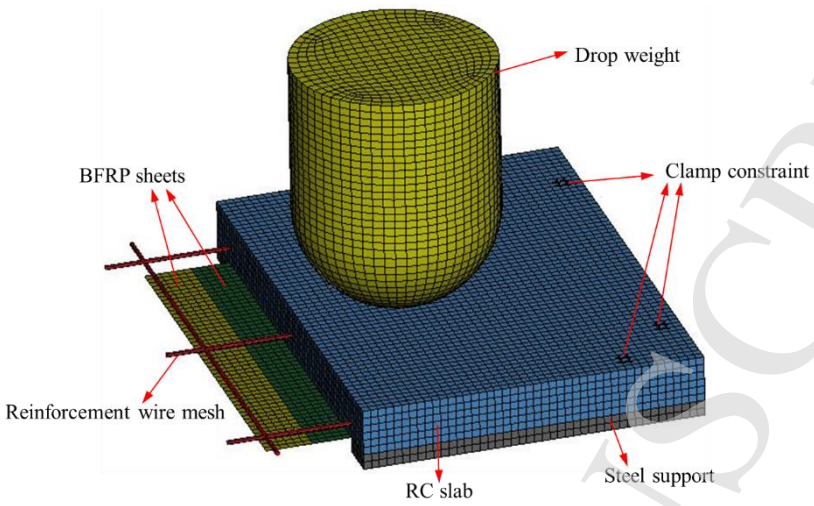

Figure 11. Numerical model of RC slab with BFRP sheet

4.2. Material model

The concrete damage model (MAT_72R3) was adopted for the concrete slab in the numerical models. The concrete model that considers shear damage, plasticity and strain rate effect has been widely used to accurately predict the dynamic behavior of concrete and concrete-like material under extreme dynamic loads [2, 28-30]. The material parameters can be generated automatically by only inputting compressive strength of concrete based on the built-in algorithm. In this study, the compressive strength of concrete was 36.4 MPa. Dynamic increase factor (DIF) was considered to predict structural responses. DIFs for concrete compressive and tensile strength [31] were used in this study. The DIF of concrete compressive strength is given as follows.

$$\mathrm{CDIF} = f_{\mathrm{cd}}/f_{\mathrm{cs}} = \begin{cases} 0.0419(\log\dot{\varepsilon}_{\mathrm{d}}) + 1.2165 & \dot{\varepsilon}_{\mathrm{d}} \le 30/s \\ 0.8988(\log\dot{\varepsilon}_{\mathrm{d}})^2 - 2.8255(\log\dot{\varepsilon}_{\mathrm{d}}) + 3.4907 & \dot{\varepsilon}_{\mathrm{d}} > 30/\mathrm{s} \end{cases} \quad (1)$$

where CDIF represents compressive dynamic increase factor, f_{cd} is the dynamic compressive strength at the strain rate $\dot{\varepsilon}_{\mathrm{d}}$, f_{cs} is the static compressive strength. The DIF for concrete tensile behavior is illustrated as follows.

$$\mathrm{TDIF} = f_{\mathrm{td}}/f_{\mathrm{ts}} = \begin{cases} 0.26(\log\dot{\varepsilon}_{\mathrm{d}}) + 2.06 & \dot{\varepsilon}_{\mathrm{d}} \le 1/s \\ 2(\log\dot{\varepsilon}_{\mathrm{d}}) + 2.06 & 1/s < \dot{\varepsilon}_{\mathrm{d}} \le 2/s \\ 1.44331(\log\dot{\varepsilon}_{\mathrm{d}}) + 2.2276 & 2/s < \dot{\varepsilon}_{\mathrm{d}} \le 150/s \end{cases} \quad (2)$$

where TDIF represents tensile dynamic increase factor, f_{td} is the dynamic tensile strength at the strain rate $\dot{\varepsilon}_{\mathrm{d}}$, f_{ts} is the static tensile strength. The piecewise linear elastoplastic model (MAT_24) was used to simulate the steel wire mesh. The yield strength and Young's modulus of the steel wire mesh were 500 MPa and 200 GPa, respectively. The DIF of steel proposed by Malvar [32] was defined along with the MAT_24 model and its equation is expressed as follows.

$$\mathrm{DIF}_{\mathrm{s/y}} = \left(\frac{\dot{\varepsilon}}{10^{-4}}\right)^{0.074-0.040\frac{f_{\mathrm{y}}}{414}} \quad (3)$$

where f_{y} is the steel yield strength in MPa. The failure strain of reinforcement is defined as 0.075 by trial and error. A rigid material (MAT_20) was used for the steel drop weight and steel support. The composite material model MAT_ENHANCED_COMPOSITE_DAMAGE (MAT_054) was used to simulate the BFRP sheets [33]. It has been used for the simulation of FRP material under dynamic loading and gives good predictions [34, 35]. The BFRP sheet had tensile strength of 1642.2 MPa, Young's modulus of 77.9 GPa, and rupture strain of 2.1%.

In addition, excessive distort and deformation of concrete elements may cause computational overflow. The distorted elements can be removed by setting material erosion algorithm MAT_ADD_EROSION, which is based on the maximum principal strain criterion. The criterion has been widely employed and reasonable results have been obtained in the previous studies of concrete structures under extreme loads [28, 36, 37]. In this study, the erosion criterion of maximum principal strain was utilized along with the concrete model MAT_72R3 to remove the damaged concrete elements that suffer large deformation in the

numerical model. In this study, the maximum principal strain was determined as 0.5 to yield good results.

4.3. Contact

Since concrete elements at the impact zone may suffer severe damage and some concrete elements might be deleted, the contact between the drop weight and the RC slab was defined by the penalty-based contact method (CONTACT_ ERODING_ SURFACE_TO_SURFACE) [33]. Moreover, as observed in the experimental results, punching shear failure may cause possible contact between the drop weight and reinforcement wire mesh, which was defined by the node to surface contact method (CONTACT_ AUTOMATIC_ NODES_ TO_SURFACE).

In the tests, the RC slab was placed over the steel support on four edges. In order to simulate the interaction between steel support and RC slab in the numerical model, a penalty-based contact algorithm (CONTACT_AUTOMATIC_SURFACE_TO_SURFACE) was employed. In addition, a penalty-based tiebreak contact algorithm (CONTACT_ AUTOMATIC_SURFACE_TO_SURFACE_TIEBREAK) was employed to simulate the bonding between the bottom surface of the RC slab and the BFRP sheets. Failure criteria were provided in the tiebreak contact with either stress-based or force-base criterion [33]. In this study, the stress-based criterion was used to model bonding failure, which is given below.

$$\left(\frac{|\sigma_n|}{NFLS}\right)^2 + \left(\frac{|\sigma_s|}{SFLS}\right)^2 \geq 1 \quad (4)$$

where σ_n and σ_s are the normal tensile stress and shear stress at the contact interface, respectively. *NFLS* and *SFLS* are input parameters that stand for the normal tensile failure stress and shear

failure stress, respectively. The failure stress was determined not only by the epoxy strength but also by the workmanship of BFRP sheets installations. Yuan et al. [38] investigated the bond behaviour between BFRP sheets and concrete by conducting single shear test and reported the peak interfacial shear stress between two layers of BFRP strips and normal concrete C40 was about 6.0 MPa. It is noted that the peak interfacial shear stress can vary depending on the quality of workmanship on BFRP sheet installation. In the numerical model, the values of NFLS (tensile failure stress) and SFLS (shear failure stress) were determined as 7.5 MPa by trial and error to achieve reasonably good agreement with the testing results of S2 and S10. This higher bond strength can also be partially attributed to the dynamic effect. It is believed that the dynamic bond strength is higher than the static bond strength owing to the strain rate effect [39 -41].

4.4. Numerical results and comparisons

The reference specimen S1 and the specimens S2 and S10 with the strengthening scheme A were employed in the numerical simulation to predict structural response. Since using anchor bolts and plates showed very limited enhancement on impact resistance of the slabs in this study, no further simulation was conducted on the slabs strengthened with anchors. The comparisons of numerical and experimental results of S1, S2 and S10 are shown in Figure 11- Figure 13. The effective plastic strain contours indicate the concrete damage level and the distribution of concrete cracks. The displacement contour is shown to compare the indentation. The failure modes of the reference specimen S1 impacted with drop height of 1.5 m are shown in Figure 11. The concrete damage was predicted around the impact zone and the G-clamps, which was

in good agreement with the observed concrete punching shear failure and cracks in the experiments. In addition, the fracture of reinforcement wire mesh at mid-span was well predicted in the numerical result. The predicted indentation dimension in the displacement contour was 430 mm, which was comparable to 440 mm in the experimental result.

Figure 12 shows the failure mode of the specimen S2, which was strengthened for the whole area subjected to the impact height of 1.5 m. Concrete damages can be observed at the impact zone on the top surface of the slab. The predicted concrete damages agreed well with the radial concrete cracks in the experiment. The specimen S10 was strengthened with the same strengthening layout as the specimen S2 but impacted with drop height of 2.0 m. The failure mode of the specimen S10 is shown in Figure 13. The numerical concrete damages were comparable with the concrete cracks in the experiment. The indentation diameter of 370 mm obtained in the numerical result was close to the measured indentation diameter of 400 mm in the tests. In addition, the fracture of wire mesh at mid-span was predicted and the debonding of BFRP sheet was well captured in the numerical simulation. The debonding failure initiated at the boundary and propagated to the centre of the slab. In general, failure modes and indentation of the RC slabs with or without BFRP strengthening strips under drop weight impact can be well predicted by using the numerical model.

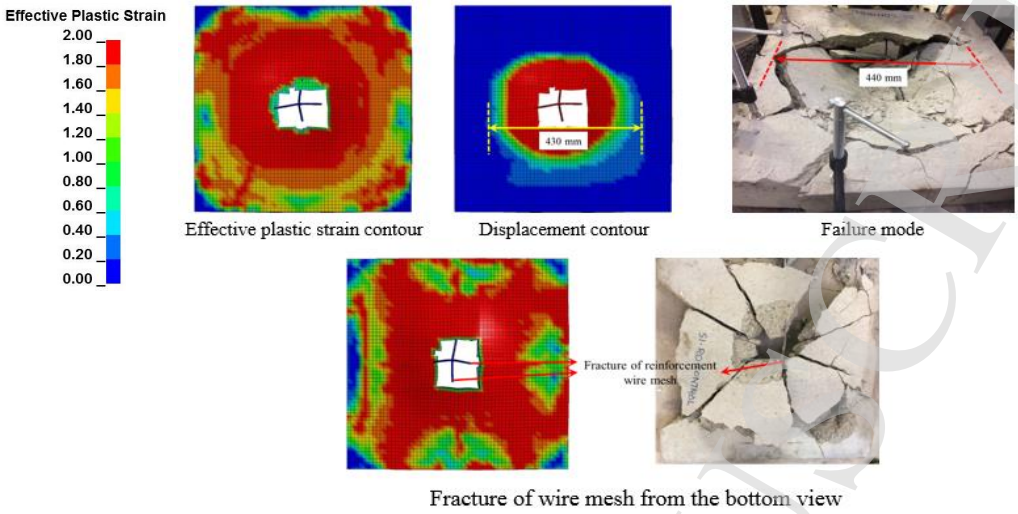

Figure 12 Numerical and experimental results (Specimen S1- 1.5m)

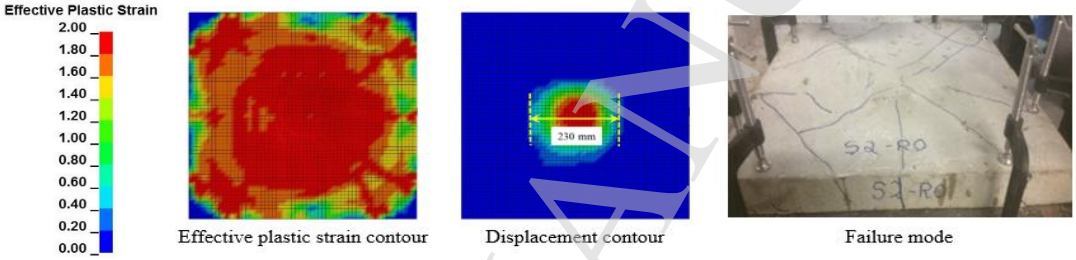

Figure 13 Numerical and experimental results (Specimen S2- 1.5m)

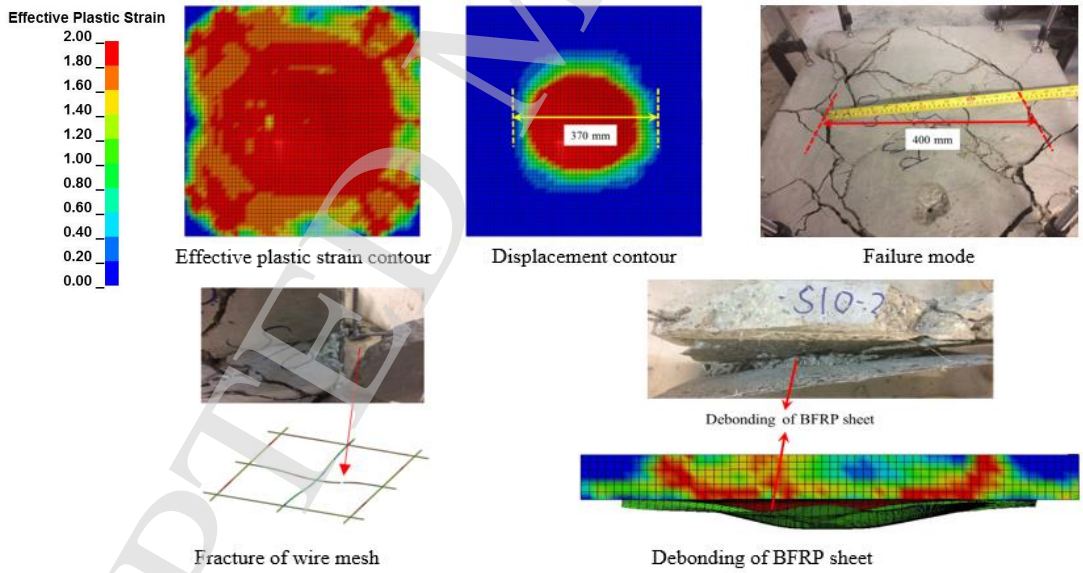

Figure 14 Numerical and experimental results (Specimen S10- 2.0 m)

Since no impact force was measured from the test, impact force time histories of three specimens were extracted from numerical results and compared in Figure 14. The maximum impact forces of S1/S2/S10 were 189.9 kN, 197.0 kN and 212.3 kN, respectively. Given the

same impact height of 1.5 m, the specimen S2 with FRP strengthening yields higher impact force than the unstrengthened specimen S1 due to the increased stiffness of slab S2. The axial stress contours of reinforcement are shown in Figure 15. The fracture failures of reinforcement in the specimens S1 and S10 were well captured by the simulation and the regions with high stress were identified in the reinforcement. Figure 16 compares the axial stress of wire mesh at the centre indicated by the circle. The points A and B in the graph represent the instances of reinforcement fracture for the specimen S1 and S10, respectively. The curve C shows the axial stress time history of specimen S2. The reinforcement was not fractured and it experienced tensile stress under impact, followed by compressive stress when slab S2 started to rebound at the centre.

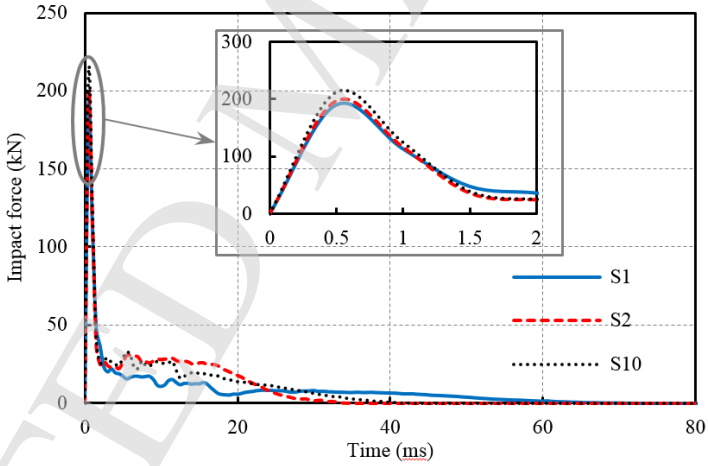

Figure 15 Time histories of impact force

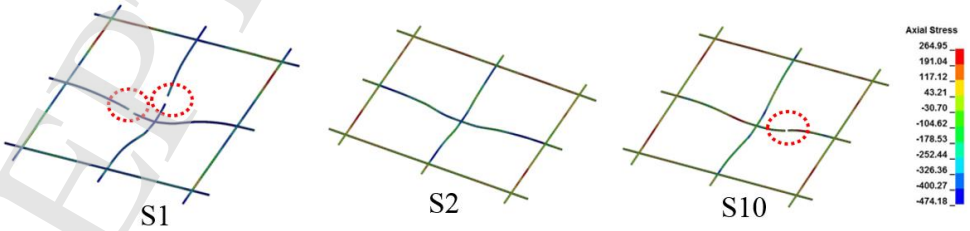

Figure 16 Axial stress contours of reinforcements

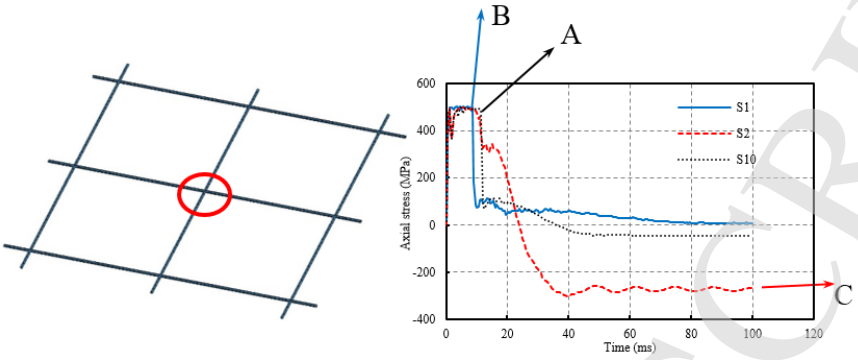

Figure 17 Comparison of axial stress of wire mesh at the centre

It can be concluded that reasonably accurate predictions of slabs under impact loads can be achieved by comparing the numerical and experimental results. With the validated numerical model of slabs with and without strengthening, intensive numerical simulations can be further carried out to predict the response of slabs by considering various dimensions, strengthening schemes and impact intensities, which are beyond the scope of this paper.

5. Conclusion

This study investigates impact resistance capacities of reinforced concrete slabs strengthened by various BFRP sheet schemes with or without anchorage systems. The main findings are summarized as follows.

(1) Using BFRP sheet can improve the impact resistance capacities of the slabs. Using 10 BFRP strips in one direction strengthening the whole area of the slab (i.e. scheme A) can significantly mitigate the damage of slabs and suppress the number and width of concrete cracks induced by impact loads. By comparing the schemes (C/E/F) using 6 BFRP strips in one direction, BFRP strips strengthening along the orthogonal direction at the centre of the slab (scheme E) demonstrated the lowest strengthening efficiency and the diagonally strengthening

scheme F showed the best performance in suppressing crack development.

(2) Anchoring BFRP sheets by using anchor bolts and plates can mitigate premature BFRP debonding but provide limited enhancement on impact resistance of the slabs in this study. The anchor holes weakened the strength of the slabs and thus reduced the strengthening efficiency.

(3) With the increasing impact energy, failure mode of RC slabs changed from global flexural failure to local punching shear failure. The premature debonding failure of BFRP sheet weakened composite actions between RC slab and BFRP sheet, resulting in severe concrete cracks of RC slabs.

(4) Numerical models were developed and verified with testing data. The failure modes of RC slabs can be well predicted by the numerical models. The impact force and axial stress of wire mesh have been numerically examined.

Acknowledgements

The financial support from Australian Research Council (ARC LP150100259) is acknowledged. Thanks are given to technician Jim Waters and former students Riya Raju and Jeoffray Singh from the University of Western Australia for the assistance during the study.

References

[1] Kaewkulchai G, Williamson E. Modeling the impact of failed members for progressive collapse analysis of frame structures. J Perform Constr Fac. 2006;20(4):375-83.
[2] Yan P, Zhang J, Fang Q, Zhang Y. Numerical simulation of the effects of falling rock's shape and impact pose on impact force and response of RC slabs. Constr Build Mater. 2018;160:497-504.
[3] Delhomme F, Mommessin M, Mougin JP, Perrotin P. Simulation of a block impacting a reinforced concrete slab with a finite element model and a mass-spring system. Engineering Structures. 2007;29(11):2844-52.

[4] Chen Y, May IM. Reinforced concrete members under drop-weight impacts. Proceedings of the Institution of Civil Engineers-Structures and Buildings. 2009;162(1):45-56.
[5] Xiao Y, Li B, Fujikake K. Experimental Study of Reinforced Concrete Slabs under Different Loading Rates. ACI Struct J. 2016;113(1):157-68.
[6] Xiao Y, Li B, Fujikake K. Behavior of Reinforced Concrete Slabs under Low-Velocity Impact. ACI Struct J. 2017;114(3):643-58.
[7] Micallef K, Sagaseta J, Fernández Ruiz M, Muttoni A. Assessing punching shear failure in reinforced concrete flat slabs subjected to localised impact loading. Int J Impact Eng. 2014;71:17-33.
[8] Zineddin M, Krauthammer T. Dynamic response and behavior of reinforced concrete slabs under impact loading. Int J Impact Eng. 2007;34(9):1517-34.
[9] Othman H, Marzouk H. An experimental investigation on the effect of steel reinforcement on impact response of reinforced concrete plates. International Journal of Impact Engineering. 2016;88:12-21.
[10] Hrynyk TD, Vecchio FJ. Behavior of Steel Fiber-Reinforced Concrete Slabs under Impact Load. ACI Struct J. 2014;111(5):1213.
[11] Othman H, Marzouk H. Impact response of ultra-high-performance reinforced concrete plates. ACI Struct J. 2016;113(6):1325-34.
[12] Bhatti AQ, Kishi N, Tan KH. Impact resistant behaviour of RC slab strengthened with FRP sheet. Mater Struct. 2011;44(10):1855-64.
[13] Yılmaz T, Kıraç N, Anil Ö, Erdem RT, Sezer C. Low-velocity impact behaviour of two way RC slab strengthening with CFRP strips. Constr Build Mater. 2018;186:1046-63.
[14] Chen W, Hao H, Jong M, Cui J, Shi Y, Chen L, Pham TM. Quasi-static and dynamic tensile properties of basalt fibre reinforcedpolymer. Composites Part B: Engineering.2017;125:123-33.
[15] Qeshta IMI, Shafigh P, Jumaat MZ. Research progress on the flexural behaviour of externally bonded RC beams. Archives of Civil and Mechanical Engineering. 2016;16(4):982-1003.
[16] Yuan C, Chen W, Pham TM, Hao H. Effect of aggregate size on bond behaviour between basalt fibre reinforced polymer sheets and concrete. Composites Part B: Engineering. 2019;158:459-74.
[17] Mahboubi S, Shiravand M. Failure assessment of skew RC bridges with FRP piers based on damage indices. Eng Failure Anal. 2019;99:153-68.
[18] Bastani A, Das S, Kenno SY. Flexural rehabilitation of steel beam with CFRP and BFRP fabrics – A comparative study. Archives ofCivilandMechanical Engineering.2019;19(3):871-82.
[19] Yuan C, Chen W, Pham TM, Hao H. Bond behavior between basalt fibres reinforced polymer sheets and steel fibres reinforced concrete. Engineering Structures. 2018;176:812-24.
[20] Jankowiak I. Analysis of RC beams strengthened by CFRP strips—Experimental and FEA study. Archives of Civil and Mechanical Engineering. 2012;12(3):376-88.
[21] Pham TM, Hao H. Review of Concrete Structures Strengthened with FRP Against Impact Loading. Structures. 2016;7:59-70.
[22] Radnić J, Matešan D, Grgić N, Baloević G. Impact testing of RC slabs strengthened with CFRP strips. Compos Struct. 2015;121:90-103.
[23] Teng J, Chen J, Smith ST, Lam L. Behaviour and strength of FRP-strengthened RC

structures: a state-of-the-art review. Proceedings of the institution of civil engineers-structures and buildings. 2003;156(1):51-62.
[24] Chen W, Pham TM, Sichembe H, Chen L, Hao H. Experimental study of flexural behaviour of RC beams strengthened by longitudinal and U-shaped basalt FRP sheet. Composites Part B: Engineering. 2018;134:114-26.
[25] Yao J, Teng J, Lam L. Experimental study on intermediate crack debonding in FRP-strengthened RC flexural members. Advances in Structural Engineering. 2005;8(4):365-96.
[26] ASTM. Standard test method for tensile properties of polymer matrix composite materials. ASTM Standards. 2008.
[27] Mutalib AA, Sivapatham S, Hao H. Experimental investigation of CFRP strengthened RC slabs with anchors under impact loading. 8th International Conference on Shock and Impact Loads on Structures2009. p. 457-65.
[28] Chen W, Hao H, Chen S. Numerical analysis of prestressed reinforced concrete beam subjected to blast loading. Materials & Design. 2015;65:662-74.
[29] Do TV, Pham TM, Hao H. Numerical investigation of the behavior of precast concrete segmental columns subjected to vehicle collision. Eng Struct. 2018;156:375-93.
[30] Wu J, Liu X, Zhou H, Li L, Liu Z. Experimental and numerical study on soft-hard-soft (SHS) cement based composite system under multiple impact loads. Mater Design. 2018;139:234-57.
[31] Hao Y, Hao H. Influence of the concrete DIF model on the numerical predictions of RC wall responses to blast loadings. Eng Struct. 2014;73:24-38.
[32] Malvar LJ. Review of static and dynamic properties of steel reinforcing bars. Materials Journal. 1998;95(5):609-16.
[33] Hallquist JO. LS-DYNA theory manual. Liver more software Technology corporation. 2006:531.
[34] Pham TM, Chen W, Hao H. Failure and impact resistance analysis of plain and fiber-reinforced-polymer confined concrete cylinders under axial impact loads. International Journal of Protective Structures. 2018;9(1):4-23.
[35] Mutalib AA, Hao H. Numerical Analysis of FRP-Composite-Strengthened RC Panels with Anchorages against Blast Loads. J Perform Constr Fac. 2011;25(5):360-72.
[36] Li H, Chen W, Hao H. Dynamic response of precast concrete beam with wet connection subjected to impact loads. Eng Struct. 2019;191:247-63.
[37] Li H, Chen W, Hao H. Influence of drop weight geometry and interlayer on impact behavior of RC beams. Int J Impact Eng. 2019; 131:222-237.
[38] Yuan C, Chen W, Pham TM, Hao H. Bond behaviour between hybrid fiber reinforced polymer sheets and concrete. Constr Build Mater. 2019;210:93-110.
[39] Yuan C, Chen W, Pham TM, Hao H, Cui J, Shi Y. Strain rate effect on interfacial bond behaviour between BFRP sheets and steel fibre reinforced concrete. Composites Part B: Engineering. 2019:107032.
[40] Yuan C, Chen W, Pham TM, Hao H, Cui J, Shi Y. Influence of concrete strength on dynamic interfacial fracture behaviour between fibre reinforced polymer sheets and concrete. Eng Fract Mech. 2020;229:106934.
[41] Yuan C, Chen W, Pham TM, Hao H, Cui J, Shi Y. Interfacial bond behaviour between hybrid carbon/basalt fibre composites and concrete under dynamic loading. Int J Adhes Adhes. 2020;99:102569.